coatings

MDPI

Article

Polymer Coatings Based on Polyisobutylene, Polystyrene and Poly(styrene-block-isobutylene-block-styrene) for Effective Protection of MXenes

Hanna Maltanava [1,*], Dmitriy Shiman [1,2], Evgeni Ovodok [1,2], Ivan Svito [3], Miraslau Makarevich [1,2], Sergei Kostjuk [1,2], Sergey Poznyak [1] and Andrey Aniskevich [4,*]

1 Research Institute for Physical Chemical Problems, Belarusian State University, Leningradskaya Str. 14, 200006 Minsk, Belarus
2 Department of Chemistry, Belarusian State University, Leningradskaya Str. 14, 220006 Minsk, Belarus
3 Department of Physics, Belarusian State University, Bobruiskaya Str. 5, 220006 Minsk, Belarus
4 Institute for Mechanics of Materials, University of Latvia, Jelgavas Str. 3, LV-1004 Riga, Latvia
* Correspondence: maltanava@bsu.by (H.M.); andrey.aniskevich@pmi.lv (A.A.); Tel.: +375-336963340 (H.M.); +371-67543303 (A.A.)

Abstract: MXene films with a conductivity of about 4000 S/cm were obtained on glass substrates following a drop-casting method and characterized by scanning electron microscopy (SEM), X-ray diffraction analysis (XRD) and Raman spectroscopy. The polymer coatings of polystyrene (PSt), polyisobutylene (PIB) and tri-block copolymer of polyisobutylene with styrene (SIBS) were deposited on MXene films and their efficiency toward the protection of MXenes against oxidative degradation was estimated at ambient conditions. A loss of conductivity was detected for PSt-coated MXene films after 220 days of storage, while pristine MXene films stored for 400 days were conductive and their resistivity increased by 2.5 times. Nonpolar polymer coatings based on polyisobutylene and tri-block copolymer of isobutylene with styrene showed ability to protect MXene films from oxidation during a long-term period. After 400 days of storage, the resistivity of the MXene films coated with PIB and SIBS increased by 1.8 and 1.4 times, respectively. The results obtained are of interest for expanding the industrial application of MXene films, increasing their operation by simple coating with nonpolar flexible polymers.

Keywords: MXene; polymer; coatings; oxidation; polyisobutylene; polystyrene; poly(styrene-block-isobutylene-block-styrene)

Citation: Maltanava, H.; Shiman, D.; Ovodok, E.; Svito, I.; Makarevich, M.; Kostjuk, S.; Poznyak, S.; Aniskevich, A. Polymer Coatings Based on Polyisobutylene, Polystyrene and Poly(styrene-block-isobutylene-block-styrene) for Effective Protection of MXenes. *Coatings* **2022**, *12*, 1477. https://doi.org/10.3390/coatings12101477

Academic Editor: Fabio Palumbo

Received: 25 August 2022
Accepted: 30 September 2022
Published: 5 October 2022

1. Introduction

MXenes are a large family of 2D layered metal carbide/nitride derived mainly through the selective etching of MAX phases with the general formula of $M_{n+1}AX_n$, where M stands for an early transitional metal (Ti, V, Mo, Ta, etc.), A is an element of IIIA and IVA groups and X is carbon and/or nitrogen, n = 1–4 [1,2]. After the etching of MAX phases, the remaining crystals are composed of loosely packed $M_{n+1}X_n$ layers, which can be easily delaminated into single- or few-layer nanosheets. Furthermore, the surfaces of MXenes are terminated by O, OH and/or F groups, which are characterized by variable composition owing to complex reactions during the etching process [3]. Given their 2D geometry and strong van der Waals forces, MXene laminates can be easily assembled into flexible films with outstanding characteristics (metallic conductivity, high specific surface area, hydrophilicity, electromagnetic and gas-sensitive properties, etc.) [4–9]. Such properties of MXene films results in promising performances in supercapacitors, Li-ion batteries, membranes, gas sensors and EMI shielding materials [8–12].

However, the poor long-term durability of MXene-based materials against oxidative degradation significantly complicates their technological processing and practical applications [13]. Several works demonstrated the oxidation of MXene nanosheets under ambient

conditions (room temperature, atmospheric oxygen) [14–17]. It has been revealed that the oxidation process of MXene started from the structural defects at the edges and extended to the basal plane of MXene flakes to form TiO_2 particles and amorphous carbon [14]. Moreover, S. Huang and V.N. Mochalin reported that MXene can be hydrolyzed in aqueous media, leading to complete transformation of 2D Ti_3C_2 MXene to titanium dioxide [18]. There are several approaches to improving the oxidation stability of MXene: synthesis of MXene particles with minimal defects, control of storage conditions for aqueous colloids of MXenes, defect passivation of MXene using organic and/or inorganic ligands, and others [13]. Although the oxidative stability of MXene flakes in solid media is higher than in colloidal suspension, MXene films are also susceptible to oxidation [15]. For pristine MXene films, annealing in a H_2 or Ar atmosphere was proposed to increase their oxidation stability [19,20].

Preparation of MXene–polymer composites is one of the promising ways to protect MXene films from oxidation and simultaneously increase their mechanical strength [21,22]. Due to the flexibility of polymers, MXene–polymer structures have exhibited optimized mechanical properties, making them feasible in various applications [23–25]. In addition, polymers can expand the interlayer spacing and prevent the aggregation of MXene nanosheets, thereby improving the durability of the composites. Up to now, a variety of MXene–polymer composites with improved performances have been investigated [26]. Nevertheless, the strategy of MXene–polymer composition is based, as a rule, on the incorporation of MXene sheets into carboxyl-, hydroxyl- and amine-containing polymer matrixes (polydopamine, poly(diallyldimethylammonium chloride), polyethyleneimine, etc.) capable of interacting with -OH groups of MXenes. To use nonpolar polymers, it is necessary to carry out a structural modification of the surface with bidentate ligands containing hydrophilic and hydrophobic groups for the incorporation of MXene into the polymer matrix [26]. Moreover, the introduction of MXenes into non-conductive polymers can result in a significant drop in electrical conductivity of the obtained MXene–polymer composites in comparison with bare MXene films [27,28]. At the same time, composites of MXene flakes with conductive polymers are not always favorable for some applications such as electronics and energy storage [29]. Despite a fairly large number of studies on the preparation of compositions with polymers [27,28,30,31], attempts to protect MXenes with nonpolar polymers by simple coating have not been described. At the same time, the strategy of polymer coating has been used for protection of other air-unstable 2D materials [32,33].

Polystyrene (PSt) is one of the most popular polymer materials for different composite nanostructures due to its optical transparency, high mechanical strength and detailed knowledge of its chemistry [34,35]. However, PSt is a rigid material which demonstrates remarkable permeability for gases, especially for oxygen. Therefore, practical interest is shifting towards flexible polymers, such as polyisobutylene (PIB) or isobutylene (Co)polymers, which exhibit excellent flexibility at ambient temperatures while being less oxygen-permeable than PSt (4.29×10^{-17}–4.71×10^{-17} $m^2 \cdot s^{-1} \cdot Pa^{-1}$ and 2×10^{-17}–8.65×10^{-17} $m^2 \cdot s^{-1} \cdot Pa^{-1}$, respectively) [36]. Moreover, commercially available copolymer of isobutylene with small amounts of isoprene (butyl rubber) has a vapor permeability $4.79 \cdot 10^{-19}$–$1.16 \cdot 10^{-18}$ $m^2 \cdot s^{-1} \cdot Pa^{-1}$ lower than most plastics [36]. Recently, moisture- and oxygen-proof PIB and poly(styrene-block-isobutylene-block-styrene) (SIBS) were used for the encapsulation of CdSe nanoplatelets and PbS quantum dots to prevent oxidation of their surfaces [37]. It has been demonstrated that PIB- and SIBS- embedded semiconductors exhibit high photo- and chemical stability.

Herein, we applied PSt, PIB and SIBS for the first time to form polymer coatings on MXene films and evaluated the effectiveness of polymers in protecting MXene from oxidative degradation. Flexible nonpolar polymer coatings based on PIB and SIBS have demonstrated the ability to increase the lifetime of MXene films under ambient conditions.

2. Materials and Methods

2.1. MAX Phase and MXene Synthesis

The Ti_3AlC_2 MAX phase was obtained by calcination of the precursors (Ti, Al and TiC) under vacuum in a high-temperature muffle furnace LHT4/18 (Nabertherm, Lilienthal, Germany). The initial powders of Ti (99.9 wt%; 325 mesh), Al (99.5 wt%; 100 mesh) and TiC (99.5 wt%; mean particle size was 2 μm) were mixed in the molar ratio of 1.0:1.1:2.0, carefully milled in an agate mortar and then pressed into tablets. Afterwards, the tablets were heated under vacuum at 1300 °C for 30 min (heating rate was 20 °C/min). The sintered tablets were crushed and milled in an agate mortar. The MAX-phase powder was sieved through a 200-mesh sieve. Then, the prepared Ti_3AlC_2 powder was etched in a solution of lithium fluoride salt (LiF) in hydrochloric acid (HCl) according to the procedure described in [2] with some modifications. In this procedure, 1 g of the Ti_3AlC_2 powder was poured into a Teflon reactor with a previously prepared solution (20 mL) consisting of 9 M HCl and 8 wt% LiF. The etching process was continued for 24 h with constant stirring at 500 rpm at 30 °C. As soon as the etching was completed, the mixture was washed with deionized water by centrifugation at 3500 rpm for 5 min to precipitate the powder and decant the supernatant. The washing cycles were repeated until the supernatant reached pH 4.5–5. The washed precipitate was collected. The multilayer MXene particles in the precipitate were then delaminated using LiCl (99.9%, Alfa Aesar, Kandel, Germany). For the delamination, the as-prepared MXene paste was placed into a Teflon reactor with 20 mL of 5 wt% solution of LiCl. The resulting suspension was stirred at 500 rpm at 30 °C for 24 h. The delaminated MXene particles were washed with deionized water by centrifugation at 3500 rpm for 10 min. The washing procedure was repeated until the supernatant reached pH 4.5–5 and green-color MXene colloidal solution was formed. The prepared delaminated MXene particles were used for preparation of a colloidal solution. The concentration of MXenes in the colloid determined by gravimetry was 5.6 g/L. The prepared stable MXene colloidal solution was purged with argon for 30–40 min and stored in a refrigerator.

2.2. Polymer Synthesis

PIB with M_n = 23,200 and M_w/M_n = 2.2 was supplied by BASF SE (Germany). PSt with M_n = 192,000 and M_w/M_n = 2.3 was purchased from Sigma-Aldrich (Darmstadt, Germany) (where M_n is the number-average molecular weight, M_w is the weight-average molecular weight, M_w/M_n is the polydispersity index).

The synthesis of SIBS was performed according to the method described in [38]. The pre-treatment of chemicals used for polymer synthesis is described in Appendix A. In the procedure, 0.2 mL of $TiCl_4$ was added to a mixture of 12.6 mL of n-hexane, 9.6 mL of CH_2Cl_2, 1.1 mL of a solution of 2,6-lutidine in n-hexane (0.1 M), 1.35 g of isobutylene (24.1 mmol) and 0.7 mL of a solution of dicumyl chloride in n-hexane (0.1 M) at −80 °C. Then, 3.5 mL of a 2 M styrene solution in a mixture of n-hexane/CH_2Cl_2 (3/2, v/v) cooled to −30 °C was poured into the mixture. The polymerization proceeded for 30 min and was terminated by pouring the reaction mixture into methanol. The resulting tri-block copolymer was purified similarly to high-molecular-weight polyisobutylene. $M_n = 65.5 \times 10^3$ and M_w/M_n = 1.4 (PIB block $M_n = 44.5 \times 10^3$ and M_w/M_n = 1.2). The ^{1}H-NMR spectrum of SIBS is presented in Appendix A (Figure A1).

2.3. Preparation of MXene Films

MXene films on glass substrates were obtained by a drop-casting method. In the procedure, 200 μL of the MXene colloidal solution (5.6 g/L) was applied on glass substrates (S = 5 cm^2) followed by drying under vacuum. Before drop-casting of the MXene colloid, glass substrates were pre-treated in a piranha solution, washed with deionized water and dried. Then, indium strips were applied to opposite sides of a glass substrate, to which copper wires were soldered.

The conductivity of the prepared films was about 4000 S/cm.

2.4. Preparation of Polymer Coating on MXene

For the preparation of polymer coatings on MXene, 350 µL of 10 wt% solution of polymer (PSt, PIB and SIBS) in toluene was drop-cast onto glass slides with the MXene films (S = 5 cm^2) with subsequent evaporation of the solvent at room temperature.

2.5. Characterization

Microstructure, surface morphology and thickness of the MXene and MXene–polymer samples were characterized using a Hitachi SU-70 scanning electron microscope with an acceleration voltage of 12 kV (secondary electron detector) and a LEO-906E transmission electron microscope. The identification of MXene structure was performed via XRD and Raman measurements. XRD analysis was carried out at room temperature using a PANalytical Empyrean diffractometer (Cu Kα radiation, step 0.02°, 2 s exposition per step over the angular range of 10–80°). Raman spectra were recorded at room temperature via a setup based on a Nanofinder HE confocal microscope (Lotis TII, Minsk-Tokyo, Belarus–Japan). Solid-state lasers were used as excitation sources (532 and 785 nm) and the excitation region diameter was about 2 µm. The power of the laser radiation incident on the sample was attenuated to a fraction of a milliwatt to avoid thermal damage of MXene. The signal accumulation time was 60 s and a cooled silicon CCD matrix was utilized as a photodetector. UV–Vis absorbance spectra of MXene colloidal solution were taken using a Shimadzu UV-2550 spectrophotometer.

Size-exclusion chromatography was performed using an Ultimate 3000 device with PLgel MIXED-C column (7.5 × 300 mm, particle size 5 µm) and one pre-column (Agilent PLgel 5 µm guard) thermostated at 30 °C, equipped with a differential refractometer. The solutions of polymers in tetrahydrofuran were eluted at flow rate of 1 mL/min. The calculation of molecular weight and polydispersity was based on polystyrene standards (Polymer Labs) with $M_w/M_n \leq 1.05$ and using the Chromeleon 7.0 program. ^{1}H-NMR spectra were recorded in $CDCl_3$ at 25 °C on a Brucker AC-500 spectrometer (Billerica, MA, USA).

2.6. Stability Test at Ambient Conditions

In the stability test, the MXene films coated with polymers on glass substrates were stored for 400 days at ambient conditions (T = 22 ± 2 °C, relative humidity (RH) = 30 ± 5%). The electrical resistance of the samples was periodically monitored using an APPA 505 True RMS multimeter (China). The relative humidity and temperature were measured by a Testo 625 (Testo SE & Co. KGaA, Titisee-Neustadt, Germany). The setup for measuring the resistance is presented in Figure A2 (Appendix A).

3. Results and Discussion

3.1. Structural and Morphological Characterization of MXene Samples

Figure 1a shows $Ti_3C_2T_x$ flakes with the lateral size of ~3 µm obtained by etching Al layers from Ti_3AlC_2 MAX phase in LiF + HCl solution. Figure 1b demonstrates the optical properties of the MXene aqueous solution. The peak of plasmon resonance is observed in the optical spectrum at 755 nm, in good accordance with previous reports for this material [1]. Moreover, the synthesized $Ti_3C_2T_x$ MXene was analyzed by XRD (Figure 2). Successful synthesis of $Ti_3C_2T_x$ MXene was proved by the absence of characteristic reflexes of the Ti_3AlC_2 MAX phase and an increase in the interlayer distance, as evidenced by the shift of the *00l* reflexes toward a lower 2θ value [2,6,7].

The SEM images of the MXene film obtained on a glass substrate are presented in Figure 3. The thickness of the obtained MXene films was about 500 nm (Figure 3a). On the surface of the MXene film, the boundaries of individual MXene flakes located in the plane of the film are clearly distinguished (Figure 3b). $Ti_3C_2T_x$ flakes are stacked on top of each other, forming a film with high conductivity.

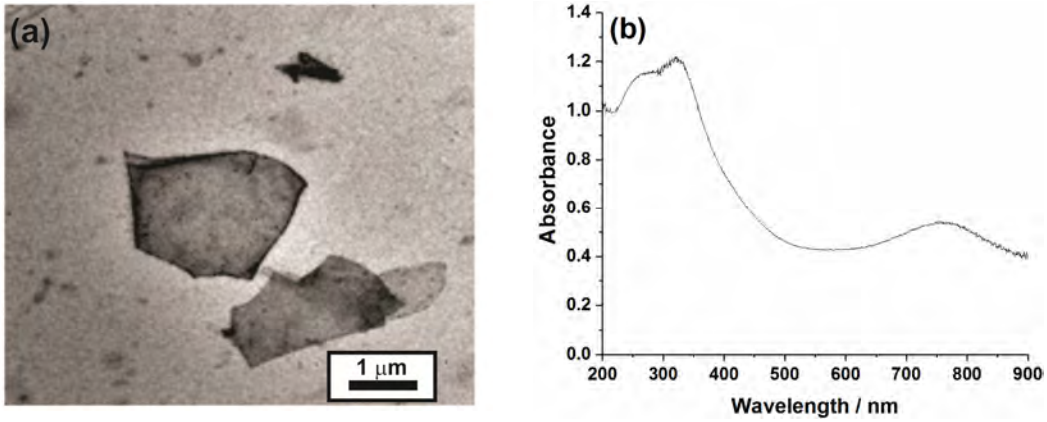

Figure 1. TEM image of delaminated $Ti_3C_2T_x$ particles (**a**) and UV–vis spectrum of freshly prepared MXene aqueous colloidal solution (**b**).

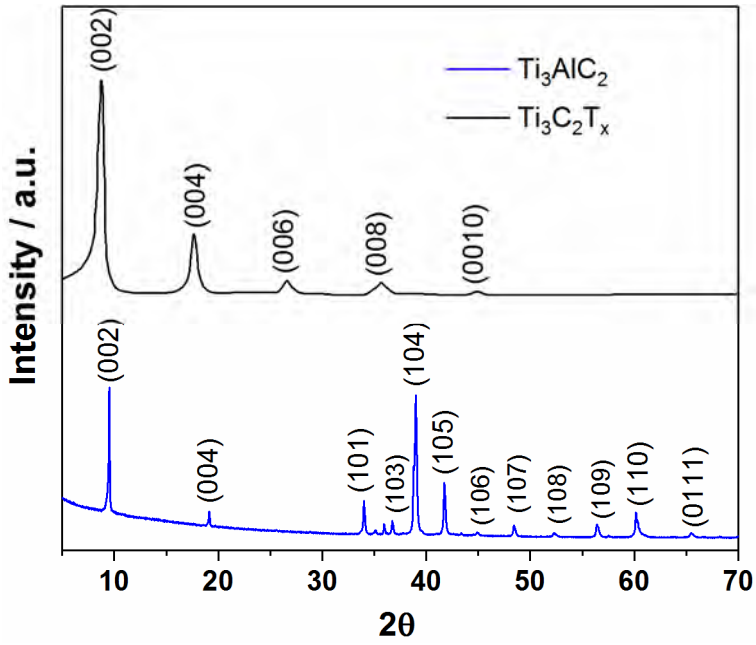

Figure 2. XRD patterns of Ti_3AlC_2 MAX phase and $Ti_3C_2T_x$ MXene.

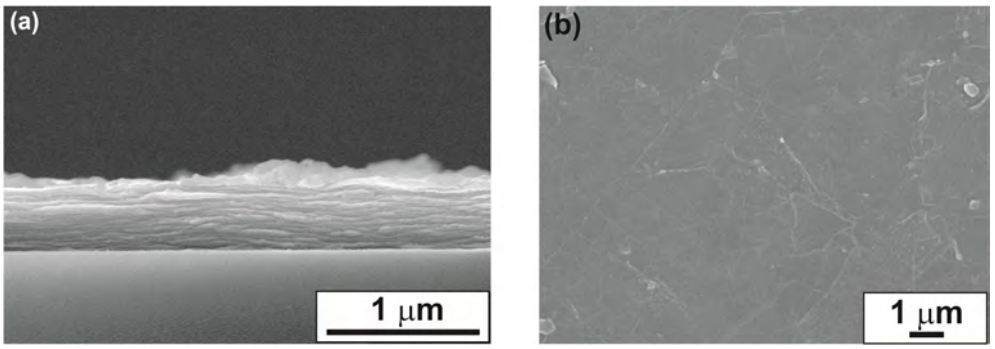

Figure 3. SEM images of MXene ($Ti_3C_2T_x$) film: cross section (**a**) and top view (**b**).

In order to analyze the structural peculiarities and surface chemistry of the obtained $Ti_3C_2T_x$ MXene films, we applied Raman spectroscopy as a sensitive tool for studies of features of 2D materials [39]. Figure 4 presents the Raman spectra of $Ti_3C_2T_x$ MXene films (where T is O, F and OH functional groups) recorded at different excitation wavelengths.

The observed peaks were deconvoluted with a Lorentz function and showed several active Raman modes (E_g and A_{1g}) characteristic for $Ti_3C_2T_x$ particles. The peak at 124 cm^{-1} is observed only when MXenes are excited with a 785 nm laser, the wavelength of which falls into the maximum of the plasmon band in the MXene absorption spectra. According to the literature data [40,41], the peaks at 198, 623 and 721 cm^{-1} are related to out-of-plane stretching vibrations of titanium and carbon atoms. The E_g modes at 255, 286 and 370 cm^{-1} can be assigned to in-plane vibrations of F, OH and O functional groups, respectively. The A_{1g} modes at 425, 514 and 586 cm^{-1} are also related to in-plane vibrations of F, OH and O groups attached to titanium atoms, respectively. The position of Raman modes does not depend on excitation laser wavelength. It should be noted that the observed Raman peaks from the MXene film are broad and overlap, which indicates a strong termination of the surface of the MXene sheets with F, OH and O groups. Moreover, the spectrum does not contain the peaks at 228 and 599 cm^{-1}, which are characteristic of Ti_3C_2 monosheets without surface termination [41]. It is also important to note that the Raman spectra of MXenes differ from those of the precursor—Ti_3AlC_2 MAX phase (Appendix B, Figure A3). In the spectrum of MAX phase, there are several sharp peaks at 182, 194 and 262 cm^{-1} and more broad peaks at 350, 575 and 632 cm^{-1}. These results are in good accordance with the data reported previously for Ti_3AlC_2 phase [42]. It can be concluded that the disappearance of the peaks at 182 and 262 cm^{-1} after etching of the MAX phase is apparently associated with the active participation of aluminum atoms in the formation of these modes.

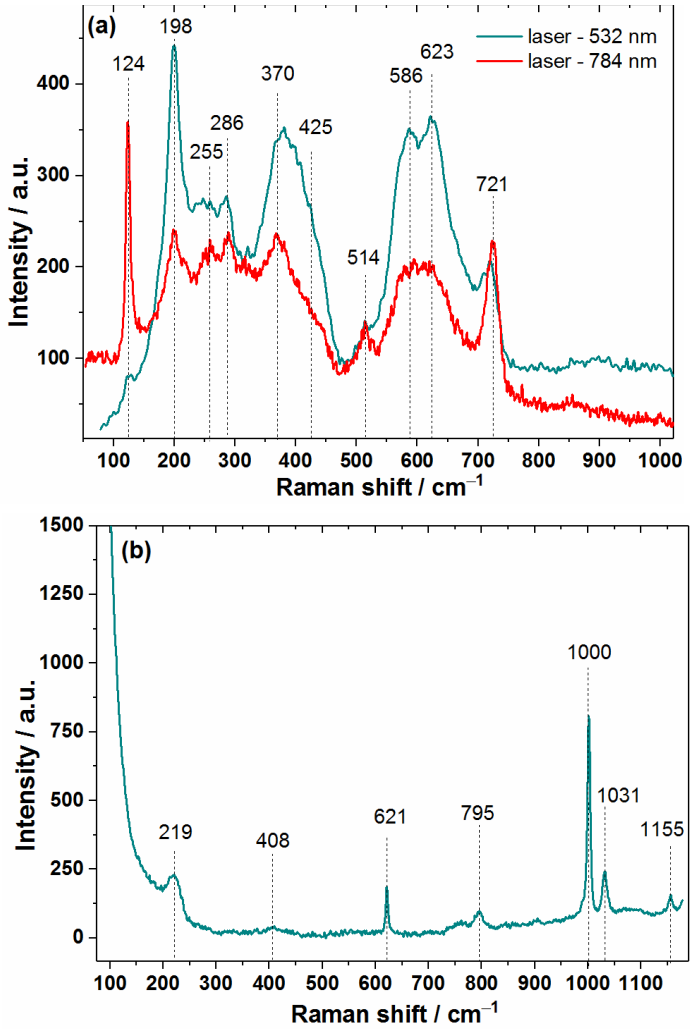

Figure 4. *Cont.*

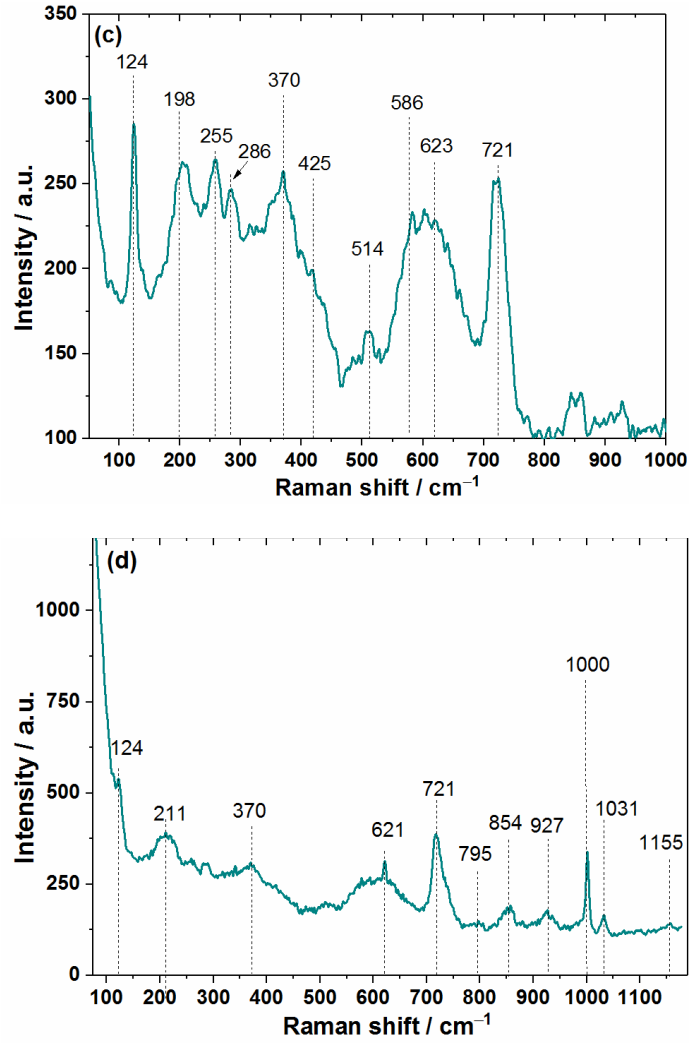

Figure 4. Raman spectra of pristine $Ti_3C_2T_x$ MXene films excited by 532 and 785 nm lasers (**a**) and polymer-coated $Ti_3C_2T_x$ MXene films excited by 785 nm laser ((**b**)—PSt-MXene; (**c**)—PIB-MXene; (**d**)—SIBS-MXene).

Figure 4b–d demonstrate the Raman spectra of polymer-coated MXene films. Raman signals from MXenes are not detected through rather thick PSt coating (Figure 4b). The observed peaks are related to principal Raman bands of PSt (621 cm^{-1} (ring deformation mode); 795 cm^{-1} (C-H out-of-plane deformation); 1000 cm^{-1} (ring breathing mode); 1031 cm^{-1} (C–H in-plane deformation); 1155 cm^{-1} (C–C stretch) and others [43]. At the same time, the principal Raman bands of MXenes have been observed in PIB- and SIBS-coated MXene films (Figure 4c,d). It is important to point out that the frequencies of Raman peaks of MXenes after PIB and SIBS deposition have not shifted, evidencing the absence of any interaction between MXenes and nonpolar polymer coatings.

3.2. Characterization of MXene–Polymer Interface

Figure 5 presents the SEM images of the MXene–polymer interface. It can be seen that the application of PSt, PIB and SIBS coatings via the drop-casting method provides good wetting of the MXene surface with polymers, i.e., the polymer coating uniformly adjoins the surface of the MXene films, and no cracks are recorded in the layer adjacent to the surface. The thickness of the applied coatings was 28 ± 2 μm.

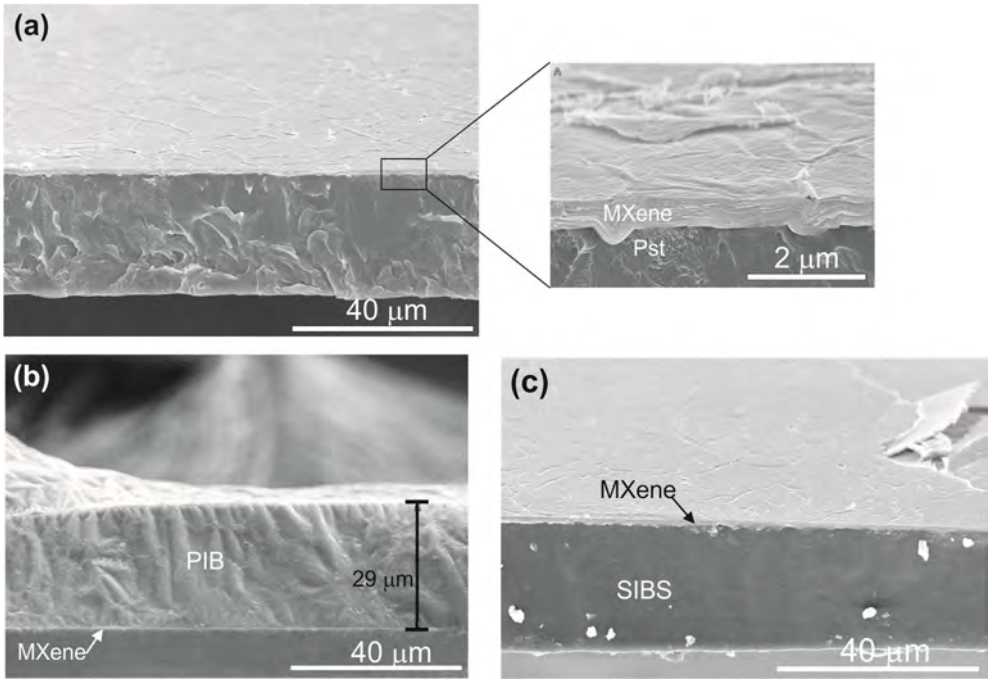

Figure 5. SEM images of MXene–polymer interface: (**a**)—MXene-PSt, (**b**)—MXene-PIB, (**c**)—MXene-SIBS.

3.3. Protection of MXene Films against Oxidation

To assess the stability of the obtained systems, we investigated the degradation of bare MXene film and polymer-coated MXene under ambient conditions (Figure 6). The degradation of MXene was monitored by a rise in the electrical resistivity of the films with time. Over 400 days, the resistivity of bare MXene films increased by ~2.5 times. As seen from Figure 6, the resistivity of PSt-coated MXene was increased significantly after 15 days of storage. The dramatic increases in R/R_0 for PSt-coated MXene can be explained by the formation of microcracks in the MXene film due to the stresses created by the PSt coating. A loss of conductivity was observed for PSt-coated MXene films after 220 days of storage. The low stability of PSt-coated MXene films can be explained by detachment of MXene–PSt layers from glass caused by the deformation of polymers (Appendix B, Figure A4). This is due to the rigidity of the PSt coating. PIB- and SIBS-coated MXene films proved to be much more stable against oxidation: after 400 days of storage, the resistivity increased by 1.8 and 1.4 times, respectively. Thus, isobutylene-based polymer coatings are more promising for the protection of MXenes against oxidation under ambient conditions. The flexibility of PIB and SIBS polymer coatings does not cause peeling of the MXene films during storage. The hydrophobicity of PIB and SIBS polymer coatings prevents diffusion of polar water molecules to the surface of MXene particles. In addition, the low oxygen permeability of PIB- and SIBS-based coatings has been previously shown [36]. Moreover, the stability test of bare MXene films and PIB- and SIBS-coated MXene under an oxygen atmosphere has additionally confirmed the low oxygen permeability of these polymers (the experimental details are presented in Appendix A).

Thus, all properties of PIB and SIBS contribute to the preservation of MXene particles in an unoxidized state. Thus, the use of PIB and SIBS allows the fabrication of layered composites based on MXene that retain the long-term stability of their electrical characteristics.

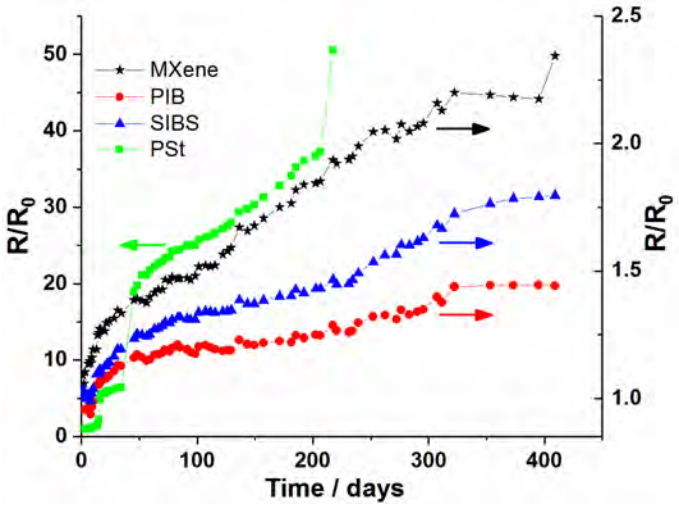

Figure 6. Temporal evolution of the relative electrical resistance R/R_0 (R_0—initial resistance values, R—monitored resistance values) for uncoated and polymer-coated MXene films stored under ambient conditions.

4. Conclusions

MXene films were deposited on glass substrates by a drop-casting method from concentrated aqueous colloids of MXene. XRD, SEM and Raman studies revealed that the prepared MXene films with a thickness of about 500 nm have layered structures formed via stacking of $Ti_3C_2T_x$ (where T is O, F and OH functional groups) flakes on top of each other. PSt, PIB and SIBS coatings were applied on MXene films, and the MXene–polymer interface was studied via SEM. It has been shown that the polymers uniformly adjoin the surface of the MXene films, and the thickness of the applied coatings was 28 ± 2 μm. The efficiency of polymer layers toward the protection of MXenes against oxidative degradation was estimated under ambient conditions. It has been shown that rigid polymer coatings, such as PSt, cause peeling of the MXene film from the substrate several days after complete drying (solvent removal) of the polymer layer. At the same time, flexible polymer coatings made of PIB and SIBS do not cause such peeling. The long-term stability testing of the electrical resistivity of bare MXene films and MXene films coated with polymers under ambient conditions demonstrated the high efficiency of PIB and SIBS coatings for MXene protection against oxidative degradation.

Author Contributions: Conceptualization, S.K. and S.P.; methodology, D.S. and S.P.; software, H.M. and I.S.; validation, S.P. and A.A.; formal analysis, H.M., S.P. and D.S.; investigation, H.M., D.S., E.O. and S.P.; resources, E.O., S.K. and A.A.; data curation, H.M., M.M. and I.S.; writing—original draft preparation, H.M. and D.S.; writing—review and editing, E.O. and S.P.; visualization, H.M., I.S. and M.M.; supervision, S.P. and A.A.; project administration, A.A.; funding acquisition, A.A. All authors have read and agreed to the published version of the manuscript.

Funding: This research was funded by the European Union's Horizon 2020 research and innovation program under the Marie Skłodowska-Curie grant agreement No. 777810, the Belarusian Republican Foundation for Fundamental Research (grants No. X20СЛИКГ-004) and the State Program for Scientific Research of Belarus "Chemical processes, reagents and technologies, bioregulators and bioorganic chemistry" (projects No. 2.1.01.03, No. 2.1.04.02).

Institutional Review Board Statement: Not applicable.

Informed Consent Statement: Not applicable.

Data Availability Statement: Not applicable.

Conflicts of Interest: The authors declare no conflict of interest.

Appendix A

The pre-treatment of chemicals utilized for SIBS synthesis

$TiCl_4$ (99.9%) was purchased from Sigma-Aldrich and was used as received. Isobutylene (99%, Sigma-Aldrich) was dried in the gaseous state by passing through an in-line gas purifier packed with BaO/Drierite and then condensed in a receiver flask at –40 °C. CH_2Cl_2 (≥99.5%, Sigma-Aldrich), n-hexane (≥95%, Sigma-Aldrich) and toluene (99.8%, Fisher) were treated with sulfuric acid, washed with aqueous sodium bicarbonate, then water, dried over $CaCl_2$, refluxed and distilled twice with CaH_2 under an inert atmosphere.

2,6-Lutinide (≥99%, Sigma-Aldrich) was dried under $CaCl_2$ and distilled with CaH_2 under reduced pressure.

Dicumyl chloride was synthesized by bubbling gaseous HCl through a methylene chloride solution of dicumyl alcohol (≥99%, Sigma-Aldrich) at 0 °C followed by recrystallization from n-hexane and drying the resulting product in vacuum.

Styrene (≥99%, Sigma-Aldrich) was treated with 10% KOH aqueous solution, repeatedly washed with water, dried under $CaCl_2$ and distilled twice with CaH_2 under reduced pressure.

^{1}H-NMR characterization of SIBS

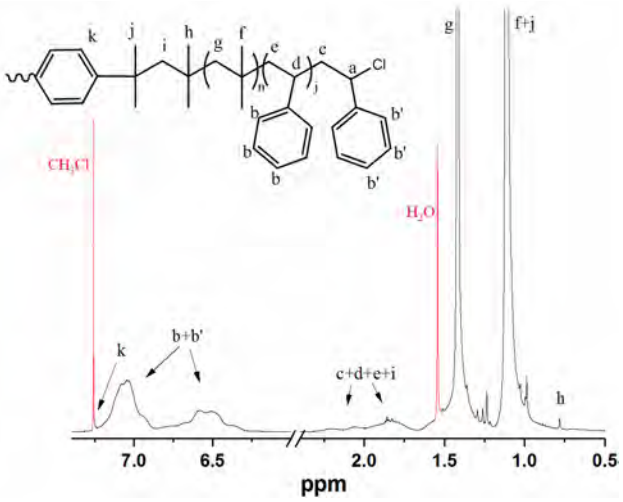

Figure A1. ^{1}H-NMR spectrum of SIBS.

The setup for resistance measurements

Figure A2. The photo of setup for resistance measurements.

Stability Test under oxygen atmosphere

In order to measure stability of bare MXenes and polymer-coated MXenes under an oxygen atmosphere, the samples were mounted onto a chamber filled with oxygen. Initially, the chamber was evacuated (up to the pressure of 2×10^{-5} bar) and then filled with oxygen (up to the pressure of 1 bar). The samples were exposed to an oxygen atmosphere for 24 h. The resistance variation of the samples was controlled by a data acquisition module (Agilent 34970A).

The storage of pristine MXene films in an O_2 atmosphere for 24 h led to an increase in R/R_0 by a factor of 1.15. At the same time, the resistance of MXene films coated with PIB and SIBS did not change, indicating a low oxygen permeability of these polymers.

Appendix B

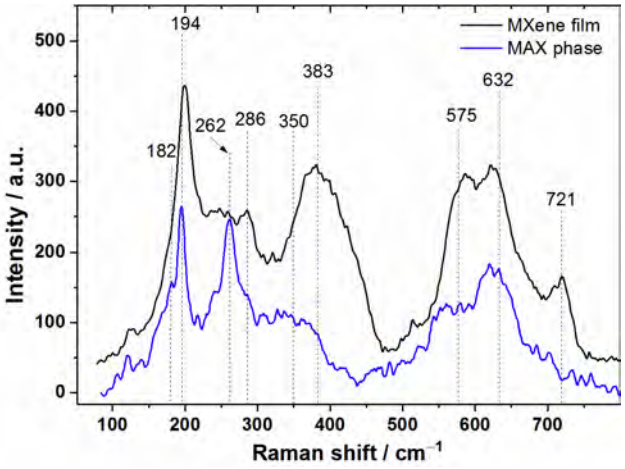

Figure A3. Raman spectra of $Ti_3C_2T_x$ films and Ti_3AlC_2 MAX phase excited with a 532 nm laser.

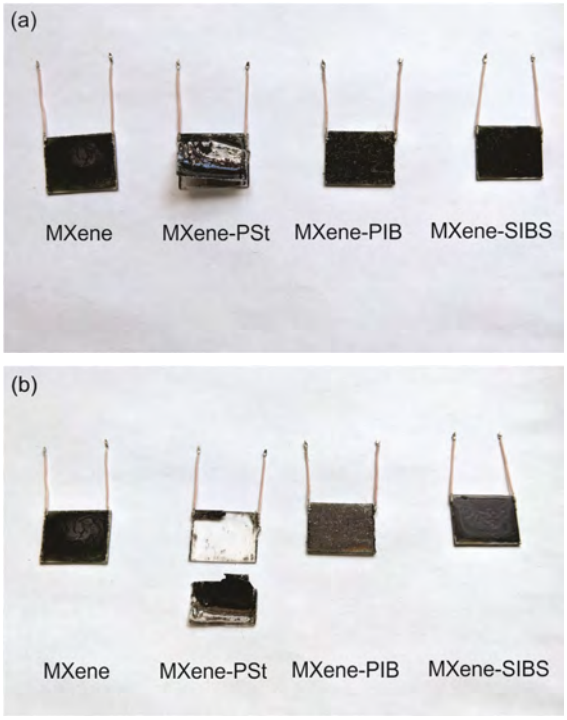

Figure A4. The photos of the samples of uncoated and polymer-coated MXene films on glass supports with contacts for resistivity measurements stored under ambient conditions over 15 days (**a**) and 220 days (**b**).

References

1. Shuck, C.E.; Sarycheva, A.; Anayee, M.; Levitt, A.; Zhu, Y.; Uzun, S.; Balitskiy, V.; Zahorodna, V.; Gogotsi, O.; Gogotsi, Y. Scalable Synthesis of $Ti_3C_2T_x$ MXene. *Adv. Eng. Mater.* **2020**, *22*, 1901241. [CrossRef]
2. Alhabeb, M.; Maleski, K.; Anasori, B.; Lelyukh, P.; Clark, L.; Sin, S.; Gogotsi, Y. Guidelines for Synthesis and Processing of Two-Dimensional Titanium Carbide ($Ti_3C_2T_x$ MXene). *Chem. Mater.* **2017**, *29*, 7633–7644. [CrossRef]
3. Murali, G.; Rawal, J.; Modigunta, J.K.R.; Park, Y.H.; Lee, J.H.; Lee, S.Y.; Park, S.J.; In, I. A Review on MXenes: New-Generation 2D Materials for Supercapacitors. *Sustain. Energy Fuels* **2021**, *5*, 5672–5693. [CrossRef]
4. Lei, J.C.; Zhang, X.; Zhou, Z. Recent Advances in MXene: Preparation, Properties, and Applications. *Front. Phys.* **2015**, *10*, 276–286. [CrossRef]
5. Gogotsi, Y.; Anasori, B. The Rise of MXenes. *ACS Nano* **2019**, *13*, 8491–8494. [CrossRef]
6. Bao, Z.; Lu, C.; Cao, X.; Zhang, P.; Yang, L.; Zhang, H.; Sha, D.; He, W.; Zhang, W.; Pan, L.; et al. Role of MXene Surface Terminations in Electrochemical Energy Storage: A Review. *Chinese Chem. Lett.* **2021**, *32*, 2648–2658. [CrossRef]
7. Ronchi, R.M.; Arantes, J.T.; Santos, S.F. Synthesis, Structure, Properties and Applications of MXenes: Current Status and Perspectives. *Ceram. Int.* **2019**, *45*, 18167–18188. [CrossRef]
8. Li, X.; Huang, Z.; Shuck, C.E.; Liang, G.; Gogotsi, Y.; Zhi, C. MXene Chemistry, Electrochemistry and Energy Storage Applications. *Nat. Rev. Chem.* **2022**, *6*, 389–404. [CrossRef]
9. Li, X.; Ran, F.; Yang, F.; Long, J.; Shao, L. Advances in MXene Films: Synthesis, Assembly, and Applications. *Trans. Tianjin Univ.* **2021**, *27*, 217–247. [CrossRef]
10. Ding, L.; Wei, Y.; Li, L.; Zhang, T.; Wang, H.; Xue, J.; Ding, L.X.; Wang, S.; Caro, J.; Gogotsi, Y. MXene Molecular Sieving Membranes for Highly Efficient Gas Separation. *Nat. Commun.* **2018**, *9*, 155. [CrossRef]
11. Kim, S.J.; Choi, J.; Maleski, K.; Hantanasirisakul, K.; Jung, H.T.; Gogotsi, Y.; Ahn, C.W. Interfacial Assembly of Ultrathin, Functional Mxene Films. *ACS Appl. Mater. Interfaces* **2019**, *11*, 32320–32327. [CrossRef] [PubMed]
12. Shahzad, F.; Alhabeb, M.; Hatter, C.B.; Anasori, B.; Hong, S.M.; Koo, C.M.; Gogotsi, Y. Electromagnetic Interference Shielding with 2D Transition Metal Carbides (MXenes). *Science* **2016**, *353*, 1137–1140. [CrossRef] [PubMed]
13. Iqbal, A.; Hong, J.; Ko, T.Y.; Koo, C.M. Improving Oxidation Stability of 2D MXenes: Synthesis, Storage Media, and Conditions. *Nano Converg.* **2021**, *8*, 9. [CrossRef] [PubMed]
14. Xia, F.; Lao, J.; Yu, R.; Sang, X.; Luo, J.; Li, Y.; Wu, J. Ambient Oxidation of Ti_3C_2 MXene Initialized by Atomic Defects. *Nanoscale* **2019**, *11*, 23330–23337. [CrossRef]
15. Habib, T.; Zhao, X.; Shah, S.A.; Chen, Y.; Sun, W.; An, H.; Lutkenhaus, J.L.; Radovic, M.; Green, M.J. Oxidation Stability of $Ti_3C_2T_x$ MXene Nanosheets in Solvents and Composite Films. *npj 2D Mater. Appl.* **2019**, *3*, 8. [CrossRef]
16. Chae, Y.; Kim, S.J.; Cho, S.Y.; Choi, J.; Maleski, K.; Lee, B.J.; Jung, H.T.; Gogotsi, Y.; Lee, Y.; Ahn, C.W. An Investigation into the Factors Governing the Oxidation of Two-Dimensional Ti_3C_2 MXene. *Nanoscale* **2019**, *11*, 8387–8393. [CrossRef]
17. Zhang, C.J.; Pinilla, S.; McEvoy, N.; Cullen, C.P.; Anasori, B.; Long, E.; Park, S.H.; Seral-Ascaso, A.; Shmeliov, A.; Krishnan, D.; et al. Oxidation Stability of Colloidal Two-Dimensional Titanium Carbides (MXenes). *Chem. Mater.* **2017**, *29*, 4848–4856. [CrossRef]
18. Huang, S.; Mochalin, V.N. Hydrolysis of 2D Transition-Metal Carbides (MXenes) in Colloidal Solutions. *Inorg. Chem.* **2019**, *58*, 1958–1966. [CrossRef]
19. Lee, Y.; Kim, S.J.; Kim, Y.J.; Lim, Y.; Chae, Y.; Lee, B.J.; Kim, Y.T.; Han, H.; Gogotsi, Y.; Ahn, C.W. Oxidation-Resistant Titanium Carbide MXene Films. *J. Mater. Chem. A* **2020**, *8*, 573–581. [CrossRef]
20. Zhao, X.; Holta, D.E.; Tan, Z.; Oh, J.H.; Echols, I.J.; Anas, M.; Cao, H.; Lutkenhaus, J.L.; Radovic, M.; Green, M.J. Annealed Ti3C2TzMXene Films for Oxidation-Resistant Functional Coatings. *ACS Appl. Nano Mater.* **2020**, *3*, 10578–10585. [CrossRef]
21. Ling, Z.; Ren, C.E.; Zhao, M.Q.; Yang, J.; Giammarco, J.M.; Qiu, J.; Barsoum, M.W.; Gogotsi, Y. Flexible and Conductive MXene Films and Nanocomposites with High Capacitance. *Proc. Natl. Acad. Sci. USA* **2014**, *111*, 16676–16681. [CrossRef] [PubMed]
22. Hatter, C.B.; Shah, J.; Anasori, B.; Gogotsi, Y. Micromechanical Response of Two-Dimensional Transition Metal Carbonitride (MXene) Reinforced Epoxy Composites. *Compos. Part B Eng.* **2020**, *182*, 107603. [CrossRef]
23. He, W.; Sohn, M.; Ma, R.; Kang, D.J. Flexible Single-Electrode Triboelectric Nanogenerators with MXene/PDMS Composite Film for Biomechanical Motion Sensors. *Nano Energy* **2020**, *78*, 105383. [CrossRef]
24. Cheng, H.; Pan, Y.; Chen, Q.; Che, R.; Zheng, G.; Liu, C.; Shen, C.; Liu, X. Ultrathin Flexible Poly(Vinylidene Fluoride)/MXene/Silver Nanowire Film with Outstanding Specific EMI Shielding and High Heat Dissipation. *Adv. Compos. Hybrid Mater.* **2021**, *4*, 505–513. [CrossRef]
25. Zheng, X.; Shen, J.; Hu, Q.; Nie, W.; Wang, Z.; Zou, L.; Li, C. Vapor Phase Polymerized Conducting Polymer/MXene Textiles for Wearable Electronics. *Nanoscale* **2021**, *13*, 1832–1841. [CrossRef] [PubMed]
26. He, S.; Sun, X.; Zhang, H.; Yuan, C.; Wei, Y.; Li, J. Preparation Strategies and Applications of MXene-Polymer Composites: A Review. *Macromol. Rapid Commun.* **2021**, *42*, 2100324. [CrossRef] [PubMed]
27. Gong, K.; Zhou, K.; Qian, X.; Shi, C.; Yu, B. MXene as Emerging Nanofillers for High-Performance Polymer Composites: A Review. *Compos. Part B Eng.* **2021**, *217*, 108867. [CrossRef]
28. Feng, A.; Hou, T.; Jia, Z.; Zhang, Y.; Zhang, F.; Wu, G. Preparation and Characterization of Epoxy Resin Filled with Ti3C2Tx MXene Nanosheets with Excellent Electric Conductivity. *Nanomaterials* **2020**, *10*, 162. [CrossRef]
29. Ali, I.; Din, M.F.U.; Gu, Z.-G. MXenes Thin Films: From Fabrication to Their Applications. *Molecules* **2022**, *27*, 4925. [CrossRef]

30. Chen, X.; Zhao, Y.; Li, L.; Wang, Y.; Wang, J.; Xiong, J.; Du, S.; Zhang, P.; Shi, X.; Yu, J. MXene/Polymer Nanocomposites: Preparation, Properties, and Applications. *Polym. Rev.* **2021**, *61*, 80–115. [CrossRef]
31. Jimmy, J.; Kandasubramanian, B. Mxene Functionalized Polymer Composites: Synthesis and Applications. *Eur. Polym. J.* **2020**, *122*, 109367. [CrossRef]
32. Tayari, V.; Hemsworth, N.; Fakih, I.; Favron, A.; Gaufrès, E.; Gervais, G.; Martel, R.; Szkopek, T. Two-Dimensional Magnetotransport in a Black Phosphorus Naked Quantum Well. *Nat. Commun.* **2015**, *6*, 7702. [CrossRef] [PubMed]
33. Li, Q.; Zhou, Q.; Shi, L.; Chen, Q.; Wang, J. Recent Advances in Oxidation and Degradation Mechanisms of Ultrathin 2D Materials under Ambient Conditions and Their Passivation Strategies. *J. Mater. Chem. A* **2019**, *7*, 4291–4312. [CrossRef]
34. Lesyuk, R.; Cai, B.; Reuter, U.; Gaponik, N.; Popovych, D.; Lesnyak, V. Quantum-Dot-in-Polymer Composites via Advanced Surface Engineering. *Small Methods* **2017**, *1*, 1700189. [CrossRef]
35. Wei, Y.; Deng, X.; Xie, Z.; Cai, X.; Liang, S.; Ma, P.; Hou, Z.; Cheng, Z.; Lin, J. Enhancing the Stability of Perovskite Quantum Dots by Encapsulation in Crosslinked Polystyrene Beads via a Swelling–Shrinking Strategy toward Superior Water Resistance. *Adv. Funct. Mater.* **2017**, *27*, 1703535. [CrossRef]
36. Le Floch, P.; Meixuanzi, S.; Tang, J.; Liu, J.; Suo, Z. Stretchable Seal. *ACS Appl. Mater. Interfaces* **2018**, *10*, 27333–27343. [CrossRef] [PubMed]
37. Shiman, D.I.; Sayevich, V.; Meerbach, C.; Nikishau, P.A.; Vasilenko, I.V.; Gaponik, N.; Kostjuk, S.V.; Lesnyak, V. Robust Polymer Matrix Based on Isobutylene (Co)Polymers for Efficient Encapsulation of Colloidal Semiconductor Nanocrystals. *ACS Appl. Nano Mater.* **2019**, *2*, 956–963. [CrossRef]
38. Makarevich, M.I.; Nikishau, P.A.; Berezianko, I.A.; Glushkova, T.V.; Rezvova, M.A.; Ovcharenko, E.A.; Bekmukhamedov, G.E.; Yakhvarov, D.G.; Kostjuk, S.V. Aspects of the Synthesis of Poly(Styrene-Block-Isobutylene-Block-Styrene) by TiCl4-Co-Initiated Cationic Polymerization in Open Conditions. *Macromol* **2021**, *1*, 243–255. [CrossRef]
39. Cong, X.; Liu, X.L.; Lin, M.L.; Tan, P.H. Application of Raman Spectroscopy to Probe Fundamental Properties of Two-Dimensional Materials. *npj 2D Mater. Appl.* **2020**, *4*, 13. [CrossRef]
40. Sarycheva, A.; Gogotsi, Y. Raman Spectroscopy Analysis of the Structure and Surface Chemistry of $Ti_3C_2T_x$ MXene. *Chem. Mater.* **2020**, *32*, 3480–3488. [CrossRef]
41. Hu, T.; Wang, J.; Zhang, H.; Li, Z.; Hu, M.; Wang, X. Vibrational Properties of Ti_3C_2 and $Ti_3C_2T_2$ (T = O, F, OH) Monosheets by First-Principles Calculations: A Comparative Study. *Phys. Chem. Chem. Phys.* **2015**, *17*, 9997–10003. [CrossRef] [PubMed]
42. Presser, V.; Naguib, M.; Chaput, L.; Togo, A.; Hug, G.; Barsoum, M.W. First-Order Raman Scattering of the MAX Phases. *J. Raman Spectrosc.* **2012**, *43*, 168–172. [CrossRef]
43. Bridges, T.E.; Houlne, M.P.; Harris, J.M. Spatially Resolved Analysis of Small Particles by Confocal Raman Microscopy: Depth Profiling and Optical Trapping. *Anal. Chem.* **2004**, *76*, 576–584. [CrossRef] [PubMed]